DSC-Vol. 58, Proceedings of the ASME Dynamics Systems
and Control Division
ASME 1996

ELECTRO-MECHANICAL TRANSDUCER FOR RAIL CAR ONBOARD POWER

Mark Nagurka, John Tabacchi, William Kaufman
Carnegie Mellon Research Institute
700 Technology Drive
Pittsburgh, PA 15230-2950
(412) 268-3100

Satoru Simizu
Advanced Materials Corporation
700 Technology Drive
Pittsburgh, PA 15230-2950
(412) 268-5650

0. ABSTRACT

This paper describes a key component of an onboard power generation system that converts mechanical vibrations into electrical power to support a train's electronically controlled pneumatic brake system. The translational generator acquires its energy from naturally occurring rail car displacements during normal train operation. The generator uses high field strength Nd-Fe-B magnets embedded in an iron-core cup assembly. When the generator is exposed to rail car vibrations, the magnet cup assembly reciprocates with respect to a copper coil. By special design of the magnet assembly, the magnetic flux lines are concentrated and made perpendicular to the coil maximizing the electrical output for a given relative displacement. In this paper the unit's design, development, and construction are reviewed. In addition, the results of laboratory testing to characterize the unit's performance as well as design considerations in meeting the vibrational energy available in a rail car environment are presented.

1. INTRODUCTION

The Association of American Railroads (AAR) is spearheading an effort to develop a Car Equipment Power System in which electrical power would be generated locally at each freight car. An important application of the power system is to support an electronically controlled pneumatic (ECP) brake system (Carlson, 1995). Other applications include powering onboard communications, inter-car communication devices, and onboard health monitoring sensors.

Electrical power to supply local power on a freight car can be obtained from several sources: *(i)* the locomotive generator using a power line running the length of the train, *(ii)* the locomotive with the addition of an onboard power storage device, or *(iii)* an onboard generator coupled to a power storage device. The first two techniques require large diameter cables running the length of the train or the use of high voltage to supply the cars with moderate power. They also rely upon intercar connectors that must survive the harsh railroad environment. To circumvent these difficulties, we have pursued an onboard power generation system that converts mechanical vibrations into electrical power.

1.1 Overview of Prototype Generator

In contrast to a typical generator in which a rotor is mounted on a bearing-supported shaft spun by a prime mover, the generator described in this paper is a translational device. The generator draws its energy from naturally occurring rail car displacements (lateral or vertical vibrations) during normal train operation. High field-strength Nd-Fe-B magnets are embedded in a special cup-shape assembly. When the generator is exposed to rail car vibrations, the magnet assembly reciprocates with respect to a copper coil, which is (indirectly) mounted to the rail car.

The generator achieves high power output as a result of tailoring the geometry and orientation of the magnets in a design that minimizes fringe effects and concentrates the magnetic flux lines in the air gap. Furthermore, the magnetic flux lines are made perpendicular to the coil maximizing the electrical output for a given relative displacement. Electromagnetic losses, due to hysteresis and eddy current effects, are inherently low in this generator. Mechanical losses are minimized by use of a low friction bearing surface on which the magnet assembly rides and by partially evacuating the internal chamber.

1.2 Background

Generator designs have been proposed and patented for producing electricity from oscillatory motions, arising from vehicle suspensions, sea waves, pedestrians and animals. Different embodiments are described, including those in which the generator uses an armature mounted on springs to generate electrical current upon relative movement between an armature and a stator (Last and Rowe, 1972) and designs utilizing a piston carrying one or more permanent magnets reciprocally driven back and forth through a coil (Wohlert and Haruch, 1978). The rocking motion of waves has been exploited to drive various mechanisms (Rich, 1970; Clark, 1981; Jacobi and Winkler, 1983).

1.3 Scope

This paper describes the development, basic operation, and results of preliminary testing of a prototype generator that operates as a linear reciprocating transducer. A detailed analytic model is developed that accounts for the mechanical and electromagnetic features of the device. Since it is desired that the device perform at maximum efficiency (suggesting operation at the mechanical resonant frequency), the dynamic performance and the frequency response is explored in detail. The model is the basis for simulation studies that lead to generator designs that meet a specified power criterion given an input excitation. The results of preliminary laboratory testing to characterize the unit's performance as well as design considerations for meeting the vibration available in a rail car environment are presented.

2. MODEL

2.1 Mechanical Systems Analysis

Consider the idealized model of the transducer connected to the rail car, as shown in Fig. 1. The transducer consists of a magnet assembly, represented by mass m, that undergoes displacement x. The assembly is connected by an equivalent stiffness, k, and an equivalent damper, b, to the rail car that has displacement y. (An expression for the equivalent viscous damping is determined in the electromagnetics analysis of Section 2.2.) Newton's second law leads to the equation of motion of the magnet assembly

$$m\ddot{x} + b(\dot{x} - \dot{y}) + k(x - y) = 0 \tag{1}$$

We are interested in the relative displacement, z,

$$z = x - y \tag{2}$$

and rewrite the equation of motion as

$$\ddot{z} + 2\zeta\omega_n\dot{z} + \omega_n^2 z = -\ddot{y} \tag{3}$$

where the natural frequency, ω_n, and damping ratio, ζ, are

$$\omega_n = \sqrt{\frac{k}{m}} \quad , \quad \zeta = \frac{b}{2\sqrt{km}} \tag{4}$$

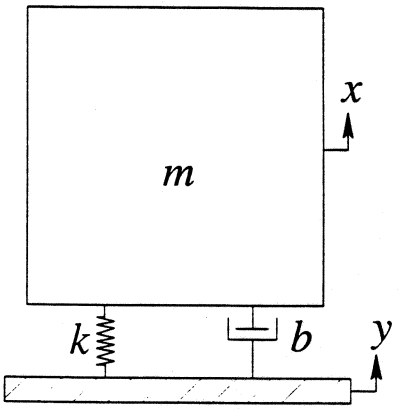

Figure 1. Model of Base Excited Structure

If the motion of the support is assumed harmonic (and unaffected by the mass-spring-damper system),

$$y = y_o \sin\omega t \tag{5}$$

with base excitation amplitude y_o and frequency ω, then Eq. (3) can be written as

$$\ddot{z} + 2\zeta\omega_n\dot{z} + \omega_n^2 z = y_o\omega^2 \sin\omega t \tag{6}$$

The steady-state solution of Eq. (6) is

$$z_{s.s.} = A\sin(\omega t + \gamma) \tag{7}$$

where A is the amplitude of relative motion,

$$A = \frac{y_o\left(\frac{\omega}{\omega_n}\right)^2}{\sqrt{\left[1-\left(\frac{\omega}{\omega_n}\right)^2\right]^2 + \left(2\zeta\frac{\omega}{\omega_n}\right)^2}} \tag{8}$$

and γ is the phase of relative motion.

At low excitation frequencies, there is no relative steady-state motion (*i.e.*, $A/y_o \ll 1$ when $\omega/\omega_n \ll 1$). At high frequencies, the relative motion is nearly equal to the displacement of the support (*i.e.*, $A/y_o \approx 1$ when $\omega/\omega_n \gg 1$). At excitation frequencies near the natural frequency, there is the opportunity for amplitude amplification in lightly damped systems. By differentiating Eq. (8) and setting the resulting equation equal to zero, it is possible to determine the condition for maximum A,

$$\frac{\omega}{\omega_n} = \frac{1}{\sqrt{1-2\zeta^2}} \tag{9}$$

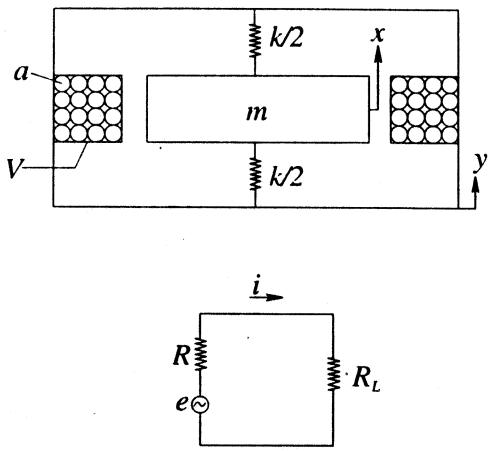

Figure 2. (a) Schematic Representation of Transducer, and (b) Electrical Circuit

2.2 Electromagnetics Analysis

Since in an electromechanical device, such as a generator, the magnetic field provides a form of coupling between the electrical and mechanical subsystems, it is necessary to augment the previous mechanical model with an electromagnetic model. By considering both electrical and magnetic effects, the analysis of this section clarifies the damping and power relationships for the generator.

The single degree-of-freedom electromechanical system is represented schematically in Fig. 2a. The figure shows the cross-section of an axisymmetric magnet assembly (indicated by mass m) in close proximity to an electrical coil. Here, the source of the damping is considered electromagnetic, due to the motion of the magnet assembly relative to the coil, and not mechanical. The *emf* is proportional to the time rate of change of the flux linkage and its direction is such as to tend to induce a current which prevents the flux from changing. In the accompanying electrical circuit of Fig. 2b, showing the generator connected to a passive resistive load, the induced voltage, e, and current, i, are

$$e = N\ell B_g \dot{z} \quad , \quad i = \frac{e}{R + R_L} \qquad (10),(11)$$

where N is the number of turns in the coil, ℓ is the length of one turn (*i.e.*, πd where d is the average diameter of the coil), B_g is the flux density available in the gap, $\dot{z}$ is the velocity of the magnet relative to the coil, R is the resistance of the coil, and R_L is the resistance of the load. In these equations, it is assumed that the self-inductance of the coil is insignificant, the leakage flux in the magnet iron is negligible, and the air gap is sufficiently narrow that the total flux flows across the gap without loss. The coil resistance, R, can be written as

$$R = \rho\frac{N\ell}{a} = \rho\frac{V\eta}{a^2} \quad , \quad \eta = \frac{N\ell a}{V} \qquad (12),(13)$$

where ρ is the resistivity, a is the cross-sectional area of the coil wire, V is the coil volume and η is the copper fraction (the ratio of the actual volume of the wire to the total volume of the coil).

The (instantaneous) output power, P, can be written as

$$P = R_L i^2 \qquad (14)$$

Substituting Eqs. (10), (11), and (12) into (14), and noting that for maximum efficiency, $R_L = R$, the power, P, can alternatively be written as

$$P = \tfrac{1}{2} b \dot{z}^2 \quad , \quad b = \frac{\eta V B_g^2}{2\rho} \qquad (15),(16)$$

where b is the equivalent viscous damping constant.[1]

By differentiating the relative displacement in steady-state given by Eq. (7) and substituting into Eq. (15), the time-averaged power, P_{av}, developed at the load is

$$P_{av} = \tfrac{1}{4} b (A\omega)^2 \qquad (17)$$

For a fixed ω_n and ζ (or, equivalently, a fixed m, b, and k), the power defined in Eq. (17) is a function only of the base excitation y_o and ω.

It is possible to present the time-averaged power in nondimensional form by introducing the normalizing power

$$P_{norm} = \tfrac{1}{4} b (y_o \omega)^2 \qquad (18)$$

where $y_o\omega$ is the amplitude of the base velocity. (P_{norm} represents the time-averaged power for the special case in which the mass is fixed in inertial space.) Then, the nondimensional power, Π, can be written as

$$\Pi = \frac{P_{av}}{P_{norm}} = \left(\frac{A}{y_o}\right)^2 = \frac{\left(\frac{\omega}{\omega_n}\right)^4}{\left[\left(1-\left(\frac{\omega}{\omega_n}\right)^2\right)^2 + \left(2\zeta\frac{\omega}{\omega_n}\right)^2\right]} \qquad (19)$$

At low damping ratios, there can be significant amplification at (and near) the frequency ratio given by Eq. (9). At high excitation frequencies (with any damping ratio), the nondimensional power Π tends to unity, and the time-averaged power P_{av} approaches P_{norm}. Since P_{norm} is proportional to ω^2, P_{av} essentially grows quadrati-

[1] The maximum efficiency in this ideal case is only 50% as indicated by the factor ½ in Eq. (15). Although higher efficiency may be achievable for a battery charging circuit with active switching and conditioning, analysis of such a system is beyond the scope of this investigation.

cally with frequency and can become quite large as the frequency increases.

For low values of ζ, the time-averaged power exhibits a local maximum. This local maximum does not occur at the same frequency ratio as that for the maximum nondimensional power. By taking the derivative of P_{av} from Eq. (17) with respect to ω and setting the resulting equation equal to zero, it is possible to show that

$$\frac{\omega}{\omega_n} = \sqrt{\delta - \sqrt{\delta^2 - 3}} \quad where \quad \delta = 2\left(1 - 2\zeta^2\right) \qquad (20)$$

is the frequency condition for the local maximum time-averaged power. Figure 3 graphically depicts this condition, and compares it to that of Eq. (9) for maximum amplitude of relative motion. From Eq. (20) it can be shown that a local maximum of the time-averaged power will occur only for $\zeta < 0.259$. For higher values of ζ there is no local maximum, and the power increases monotonically with increasing excitation frequency.

By substituting Eq. (20) into (19), the nondimensional power can be written as a function of ζ. This relationship, giving the condition for local maximum time-averaged power, is portrayed in Fig. 4. Smaller values of ζ, or, equivalently, larger values of Π, correspond to increasing peaking of the time-averaged power (at the local maximum), indicating a system design highly tuned to the excitation frequency. For values of ζ near 0.259, or $\Pi \approx 3$, the time-averaged power *vs.* frequency plot is approximately flat at the excitation frequency, denoting a less selective yet more broadband design.

2.3 Simplified Analysis

An approximate design of the generator can be achieved by simplifying the preceding equations. This simplified analysis starts with either Eq. (9), specifying the frequency ratio for maximum amplitude of relative motion, or Eq. (20), giving the frequency ratio for local maximum time-averaged power. For both equations, a small ζ corresponds to $\omega/\omega_n \cong 1$. (For example, for $\zeta = 0.2$ the ratio $\omega/\omega_n = 1.04$ in Eq. (9) and $\omega/\omega_n = 1.10$ in Eq. (20).) It follows that the relative amplitude, A, of Eq. (8) can be approximated as

$$A \cong \frac{y_o}{2\zeta} \qquad (21)$$

and the time-averaged power, P_{av}, from Eq. (17) can be written as

$$P_{av} \cong \frac{b}{16}\left(\frac{y_o\omega}{\zeta}\right)^2 \qquad (22)$$

both of which hold under the assumption of small ζ.

These simplified equations provide several interesting insights. For example, for a given P_{av}, b, and ζ (*i.e.*, desired power and specified system), there is a "tradeoff" between excitation amplitude y_o and frequency ω since the product $y_o\omega$ is approximately constant. Thus, in an application where the input frequency is low, the amplitude must be sufficiently high to achieve a specified power. Another finding is the importance of mass, m, in meeting a power specification when the input frequency is low. This result can be demonstrated by noting that, for a fixed b, the product km must be high to achieve a small ζ and the ratio k/m must be small to ensure a small $\omega \cong \omega_n$ (see Eqs. (4)). For both conditions to be satisfied, m must be sufficiently high.

3. GENERATOR DESIGN

The design objective is to deliver $10W$ of power. ($5W$ will be used to power ECP brakes and $5W$ will charge a battery.) A unique feature of the design is the magnet assembly, the topic of the first subsection. Following subsections demonstrate how the analytical development can be applied, and provide details associated with the mechanical design of the prototype unit.

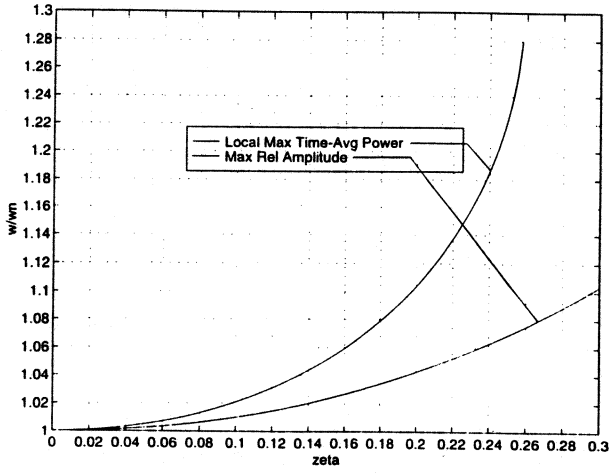

Figure 3. Frequency Ratio vs. Damping for Maximum Relative Motion and Local Maximum Time-Averaged Power

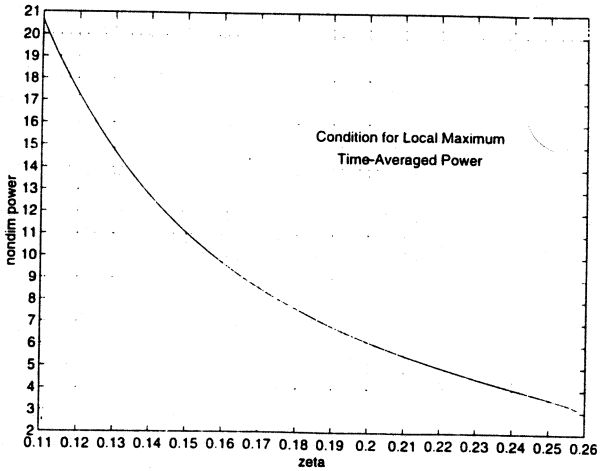

Figure 4. Nondimensional Power vs. Damping Ratio for Local Maximum Time-Averaged Power

3.1 Magnet Design

Equations (15) and (16) indicate that, for a given $\dot{z}$, the output power P of the generator is maximized by maximizing the quantity $\eta V B_g^2/\rho$. The copper fraction η is dictated by the coil design. Copper is the only practical choice to minimize the electrical resistivity ρ. This leaves the coil volume (actually, volume of electromagnetic interaction space, or gap volume) V and the flux density B_g for electromagnetic optimization. It is noted that the term $VB_g^2 \approx \mu_o V_m (BH)_{\max}$ where μ_o is the permeability of air, V_m is the magnet volume and $(BH)_{\max}$ is the maximum energy product. For a Nd-Fe-B magnet, currently the highest field-strength magnet available, $(BH)_{\max}$ is approximately $300 kJ/m^3$ ($37.5 MGOe$), or approximately ten times the energy product of a ferrite magnet.

Magnetic circuit designs that maximize VB_g^2 were explored. A cup shape design, shown in cross-section in Fig. 5, was selected because it utilizes the limited space effectively by focusing the flux from the bottom and ring magnets into an annular gap. The cup serves as the outer return path in the magnetic circuit.

A two-dimensional finite element analysis method was employed to calculate the average flux density in the gap. To determine the optimal design, the calculation was repeated with different aspect ratios while keeping the total volume constant. The effects of material parameters were also examined by varying the remanence and coercivity of the permanent magnet and the saturation induction of the soft magnet material.

In the final analysis, it was found that over the gap volume of $1.23 x 10^{-4} m^3$ the average value of B_g was $0.47T$ using a permanent magnet with a remanence of $1.2T$ and a maximum energy product of $288 kJ/m^3$ ($36 MGOe$) and a soft magnetic material with a saturation induction of $1.9T$. The result agrees well with the measured value for the actual prototype as summarized in Table 1. The flux distribution in this final design, presented in Fig. 6, shows that the flux lines are perpendicular in the gap for the coil.

Table 1. Parameters of Coil and Magnet Design

Description	Symbol	Value	Units
Copper Fraction	η	0.4	–
Coil Volume	V	$1.2 x 10^{-4}$	m^3
Flux Density Available in Gap	B_g	0.5	*tesla*
Resistivity of Coil Wire	ρ	$2.0 x 10^{-8}$	*ohm-m*
Coil Resistance	R	114	*ohm*

In the implementation, a single magnet disk is used for the bottom magnet, and the magnetic ring is built up of sector magnets. As indicated in Fig. 5, the sector magnets are magnetized with north oriented radially inward, whereas the disk magnet has north pointed up along its axis. The magnets are arranged such that they line the inner wall and bottom portion of a magnetic steel cup and surround a cylindrical magnetic steel inner core. The combination of the inner core, magnets, and cup – referred to in this paper as the magnet assembly – represents a sprung mass in the generator design.

3.2 Design Calculations

The design of this first prototype serves as a "proof of concept" and validation of the analytical methods. The parameters of Table 1 represent the coil and magnet design, and give $b = 300 \frac{N \sec}{m}$ from Eq. (16). For this first prototype, the input environment is assumed to be $y_o = 1.5 mm$ at $\omega = 20 Hz$ and the desired power specification is $P_{av} = 10 W$. (The excitation input in a rail car environment is discussed in Section 4.1.)

A procedure follows for designing the generator, *i.e.*, specifying the mass of the magnet assembly and the stiffness of the magnet support. A premise of the design solution is interest in placing the local maximum of the time-averaged power at the excitation fre-

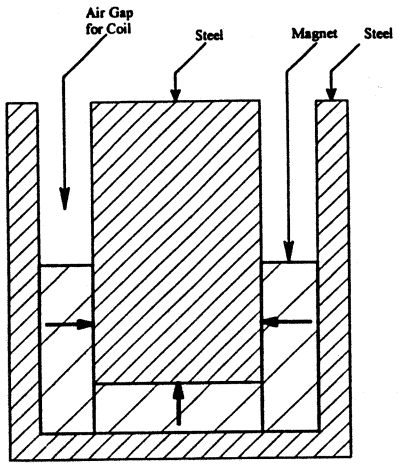

Figure 5. Cross-Section of Magnet Assembly

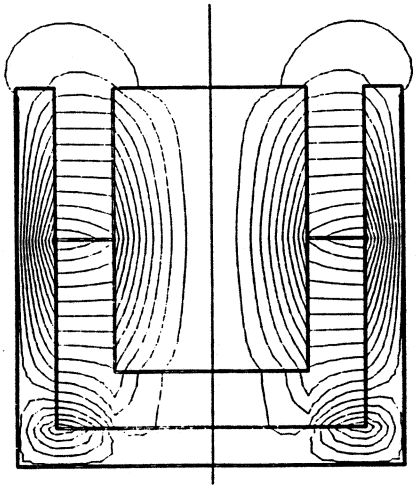

Figure 6. Magnetic Flux Lines in Magnet Assembly

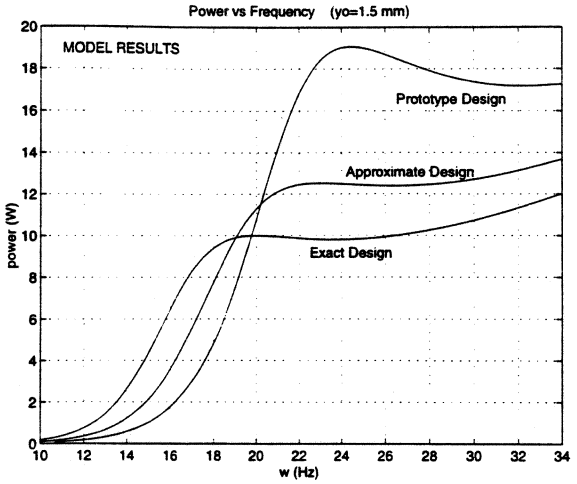

Figure 7. Power vs. Frequency: Model Results

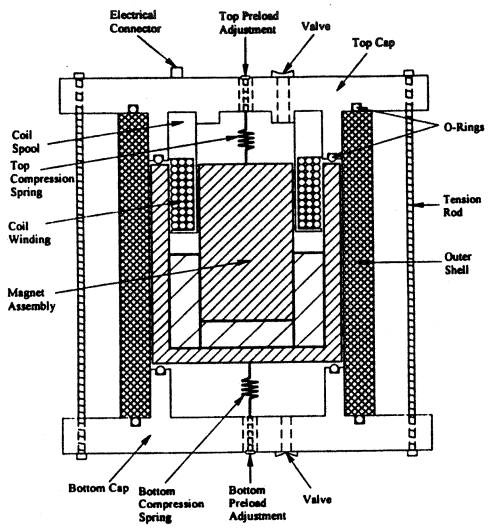

Figure 8. Cross-Section of Prototype Generator

quency. From b and the excitation input characteristics, the normalizing power is calculated from Eq. (18) giving $P_{norm} = 2.67W$. Since the desired time-averaged power $P_{av} = 10W$, the nondimensional power $\Pi = 3.75$ from Eq. (19). From Fig. 4, this nondimensional power can be achieved with a $\zeta = 0.247$. At this damping ratio, $\omega/\omega_n = 1.21$ is the condition for local maximum power from Fig. 3, and, thus, $\omega_n = 16.5\,Hz$ given the excitation frequency $\omega = 20\,Hz$. With ζ and ω_n known, it is possible to determine the values of m and k from Eqs. (4), *i.e.,* by rearrangement $m = b/2\zeta\omega_n = 5.86kg$ and $k = b\omega_n/2\zeta = 63{,}000\frac{N}{m}$.

This "exact" design can be compared with that of the simplified analysis of Section 2.3. Under the approximation $\omega_n = \omega$, Eq. (22) can be solved for ζ giving $\zeta \cong 0.258$, and then the values $m \cong 4.63kg$ and $k \cong 73{,}100\frac{N}{m}$ can be found from Eqs. (4). The disparity between this approximate solution and the above "exact" solution can be attributed to the fact that the key assumption of the simplified analysis, namely a small ζ such that $\omega_n \approx \omega$, is not adequately met. (The discrepancy at the predicted ζ is evident in Fig. 3.)

For the prototype design the mass of the magnet assembly is $m = 5.0kg$ and the support element stiffness is $k = 90{,}000\frac{N}{m}$. These system parameter values correspond to a natural frequency $\omega_n = 21.35Hz$ and a damping ratio $\zeta = 0.224$. For this design, the local maximum of the time-averaged power occurs at $24.5Hz$. The time-averaged power as a function of frequency is shown in Fig. 7 for the prototype design, the approximate design, and the "exact" design. Assuming an input of $1.5mm$ at $20Hz$ the predicted power for the prototype design meets the specification of $10W$. One feature of the power curves is the relatively "broad-band" nature of the design, *i.e.,* the power is approximately constant over a wide frequency range.

3.3 Generator Prototype

This section focuses on the design and construction of a working prototype. The generator, shown in cross-section in Fig. 8, consists of four main components: the coil assembly (coil spool and winding), the magnet assembly, the housing (outer shell), and the end caps (top and bottom). Additional components include the top and bottom springs, O-ring stops and seals, valves, electrical connector, and tension rods.

For ease of assembly, the outer shell consists of a low friction (Delrin) cylinder in which the outer surface of the magnet assembly rides. The coil (spool) is mounted integrally into the top cap. The top and bottom caps contain a locating seat for compression springs which are preloaded to center the magnet assembly. The travel of the magnet assembly is limited by hard stops built into the top and bottom caps. These hard stops are lined with O-rings serving as bumpers. The top and bottom caps also contain O-rings, which are used to provide a seal with the outer shell. In addition, valves at the top and bottom caps serve as vacuum access ports to evacuate the inner chamber. The top cap contains an electrical feed-through connector. The device is easily assembled using four tension rods that lock the top and bottom caps securely to the shell.

3.4 Full System Design

The full onboard power system is comprised of three main components: the electro-mechanical transducer (*i.e.,* the generator), an electronics package (power conditioning and charging circuitry), and an energy storage device. The electronics package includes a power conditioning circuit and a charging circuit. The energy storage device is a $12VDC$ sealed lead acid battery.

The output of the generator, which produces unregulated, alternating current, is rectified and filtered in a conditioning circuit. The resulting DC signal is passed to a charging circuit, which monitors the battery charge state. When the battery is fully charged, power is dissipated in a dummy load to maintain constant damping on the

generator. The battery is responsible for handling the power demand as needed (*i.e.*, the battery handles surges during normal operation.)

The generator, battery and electronics package are assembled in a sealed (water-tight) rectangular enclosure. The output of the prototype assembly is connected to the load (ECP brake system) through a single vibration-resistant electrical power connector. The weight of the complete system prototype is $24.3kg$ ($53.5lb$). The external dimensions are: $41cm$ ($16in$) height, width $23cm$ ($9in$), and depth $23cm$ ($9in$).

3.5 Preliminary Testing

Preliminary testing of the prototype generator on a mechanical shaker table has been conducted. In these tests, the travel of the shaker table was $\pm 1.92mm$, and the current through a constant load resistance $R_L = 102\Omega$ was monitored. The results for delivered power, presented in Fig. 9, show that effects of air compressibility in the chamber are important. As the vacuum pressure increases there is strong trendwise agreement with the prototype model predictions. Air compressibility and damping degrade the performance of the prototype device, and contribute to the smaller than anticipated power output.

4. REAL-WORLD CONCERNS

The generator must survive a rail car environment that is harsh in terms of high accelerations, temperature extremes, wide humidity range, *etc.* The following section examines one "real-world concern," namely, characterizing the driving input to the generator for the rail car application. Other concerns are relegated to future studies.

4.1 Rail Car Environment

The vibration environment of railway vehicles has been the subject of previous studies (Kenworthy, 1978; Haque, *et al*, 1991), motivated primarily by interest in reducing damage during the transport of vibration sensitive cargo, such as electronic equipment and precision machinery. The results of past investigations suggest that the severity of the vibration environment is strongly dependent on the type of vehicle, the speed of operation, the track conditions, and the characteristics of the cargo.

In general, the suspension of most rail freight cars has a bounce natural frequency of about $2Hz$ with the car loaded and about $4Hz$ with the car empty. The pitch natural frequencies are approximately the same as those for bounce, and in roll the natural frequency is about $0.7Hz$ with the car loaded. Torsional and bending modes of the car body range from $2Hz$ to $10Hz$ or beyond. Flat cars are the "floppiest," while tank cars are quite stiff.

In the Fall 1995 AAR participated in a test of an electro-pneumatically equipped double stack train running from Chicago to Los Angeles during which data of car body vertical accelerations were

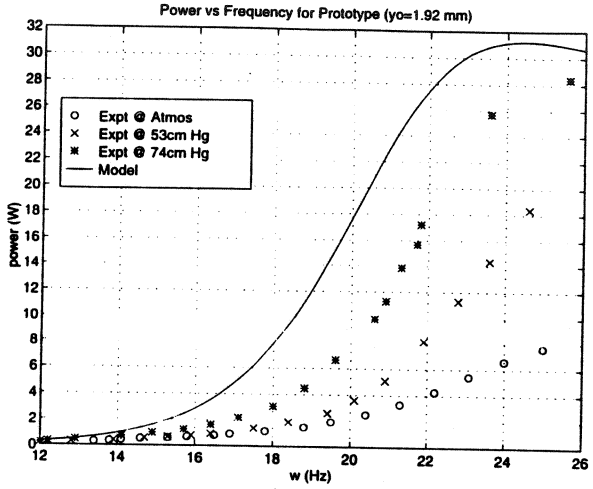

Figure 9. Power vs. Frequency for Prototype Design

collected. Bursts of data for cases in which the vertical acceleration exceeded $\pm 0.6g$ were stored. Each burst consisted of 20 seconds of real-time data, collected at a rate of 128 samples/second.

To utilize this time-based data, it is necessary to extract its frequency content. The *rms* acceleration in one-third octave bands has been calculated for a sample burst, and it exhibits several peaks, including modes at $3.16Hz$, $12.8Hz$, $20.4Hz$, and $31.1Hz$. The corresponding displacement amplitudes are small (*e.g.*, $1.38mm$ at $3.16Hz$), and the results suggest that there is not significant vibrational energy in the car body. It should be noted, however, that the acceleration measurements were taken at a single point in the car body (located on the midcenter line of the car body floor) and do not necessarily represent a point at which the acceleration is maximum. It is reasonable to expect significantly larger displacement amplitudes at points far from the midcenter line and high in the car body, where there would be contributions due to angular motions (roll, pitch, and yaw).

4.2 Design Options for Rail Car Environment

This subsection explores candidate designs that may be better matched to the vibrational characteristics of the rail car environment. As before, it is assumed that for the coil and magnet design the parameters of Table 1 apply, giving $b = 300\frac{N\sec}{m}$ from Eq. (16). Here, in comparison to the prototype design, the input amplitude is increased and the frequency is lowered, *i.e.*, the rail car environment is assumed to be $y_o = 5mm$ at $\omega = 3Hz$. Thus, the normalizing power is $P_{norm} = 0.666W$.

For the first redesign, the desired time-averaged power is kept at $P_{av} = 10W$, giving the nondimensional power $\Pi = 15.0$ from Eq. (19). From Fig. 4, this nondimensional power corresponds to $\zeta = 0.129$ and then from Fig. 3 (or Eq. (20)), $\omega/\omega_n = 1.036$, implying $\omega_n = 2.896\,Hz$ for the known excitation frequency $\omega = 3\,Hz$. With ζ and ω_n determined, the values of m and k from

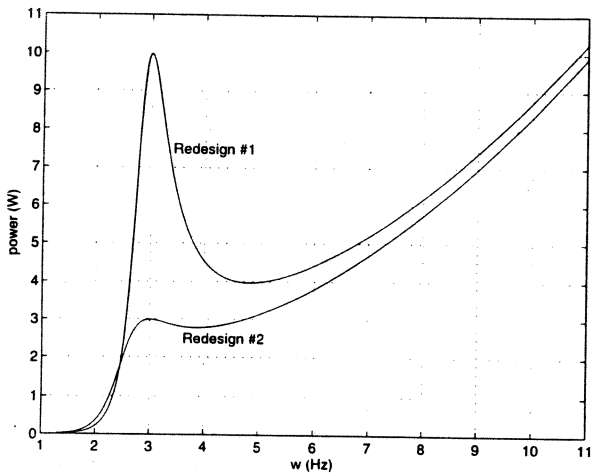

Figure 10. Power vs. Frequency for Redesign Cases

Eqs. (4) are m=63.9kg and $k = 21{,}150\frac{N}{m}$. In this design, there is a significant increase in mass in comparison to the prototype design.

The time-averaged power for this case, called Redesign #1, as a function of frequency is shown in Fig. 10. The desired power of $10W$ is met at $3Hz$, and there is significant peaking about this frequency due to the low ζ. The high selectivity of this design makes it most appropriate for applications in which the input vibration is characterized by a single frequency that is not changing.

Another design has also been explored. Here the input environment is the same, but the desired power has been reduced to $P_{av} = 3W$, giving a nondimensional power $\Pi = 4.5$. For this case, called Redesign #2, $\zeta = 0.23$, $\omega_n = 2.586\,Hz$, $m = 40.1kg$, and $k = 10{,}600\frac{N}{m}$. The power as a function of frequency, shown in Fig. 11, indicates that the desired power of $3W$ is met at $3Hz$, and that this is a relatively broad-band design. This design is a better choice for applications in which the input frequency is not perfectly known and/or is subject to variability.

It is clear that mass is a key element in designing the generator for lower frequency input situations. It is also evident that the designs may be made highly selective to an input frequency, if it is well known and stable, or made "broad-band" for situations – such as with rail car vibration – in which the input is not a single fixed frequency.

5. SUMMARY

This paper describes activities toward the development of a prototype generator designed to provide local electrical power on a rail freight car to power electro-pneumatically controlled brakes. The device utilizes the car motion to drive a translating oscillating magnet, which then generates current in a concentric pickup coil. A unique feature of the generator is the magnet assembly that, by design, concentrates the magnetic flux lines in the gap and increases efficiency. Other noteworthy features are: *(i)* The concept exploits naturally occurring (and otherwise lost) motion of the car as the driving force. *(ii)* The generator is self-contained, with no externally moving parts. *(iii)* The device is easy to assemble/disassemble, and is potentially very rugged. *(iv)* The unit has broad latitude for installation location, and requires no inter-car power connections.

The paper develops an analytic model that captures both the mechanical and electrical features of the reciprocating generator. The model has been exercised to explore overall feasibility issues and to suggest candidate designs. Based on the model, one such design has been constructed and tested.

6. ACKNOWLEDGMENTS

The authors gratefully acknowledge the financial and technical support of the AAR. The authors wish to thank Mr. John Peters and Mr. Shahram Mehrvarzi (both of AAR) for their help as technical liaisons, Mr. John Wiss (CMRI and Mechanical Engineering, CMU) for his design and technical contributions, Mr. James Dillinger and Mr. Daniel McKeel (both of the Mechanical Engineering Machine Shop, CMU) for their machining expertise, and Mr. Jeff Hibner (CMRI) for his help in the prototype construction.

7. REFERENCES

Carlson, F.G., 1995, "Freight Car Computer Controlled Electronic Brake Systems," *Rail Transportation 1995*, ed. R. Newman, ASME IMECE, San Francisco, CA, RTD-Vol. 10, pp. 11-22.

Clark, S.J., 1981, "Apparatus for Generating Electricity," U.S. Patent 4,291,234, Sep 22, 1981.

Haque, I., Law, E.H., Fries, R.H., and Figliola, R.S., 1991, "Prediction of Vibration Environment During Rail Transport: A Case Study," ASME Winter Annual Meeting, Paper WAM-91-WA-SERA-2.

Jacobi, E.F. and Winkler, R.J., 1983, "Wave Motion Electric Generator," U.S. Patent 4,423,334, Dec 27, 1983.

Kenworthy, M., 1978, *Test Results Report, Piggyback Evaluation Project, Volume I: Characterization of Vibration Environment*, Technical Report FRA/ORD-79/05.

Last, J.D and Rowe, D.N.E., 1972, "Method of Generating Electricity and Electrical Generator," U.S. Patent 4,191,893, Oct 3, 1972.

Rich, A.H., 1970, "Oceanographic Generator," U.S. Patent 3,546,473, Dec 8, 1970.

Wohlert, A.M. and Haruch, J., 1978, "Illuminated Fishing Lure," U.S. Patent 4,114,305, Sep 19, 1978.